NASA TECHNICAL NOTE

NASA TN D-6614

NASA TN D-6614

CALCULATION OF LAMINAR HEAT TRANSFER TO THE WINDWARD SURFACES OF STRAIGHT WING SHUTTLE VEHICLES AT HIGH ANGLE OF ATTACK AND WITH YAW

by C. C. Pappas

Ames Research Center
Moffett Field, Calif. 94035

NATIONAL AERONAUTICS AND SPACE ADMINISTRATION • WASHINGTON, D. C. • MAY 1972

1. Report No.	2. Government Accession No.	3. Recipient's Catalog No.
NASA TN D–6614		

4. Title and Subtitle	5. Report Date
CALCULATION OF LAMINAR HEAT TRANSFER TO THE WINDWARD SURFACES OF STRAIGHT WING SHUTTLE VEHICLES AT HIGH ANGLE OF ATTACK AND WITH YAW	May 1972
	6. Performing Organization Code
7. Author(s)	8. Performing Organization Report No.
C. C. Pappas	A-4196
	10. Work Unit No.
9. Performing Organization Name and Address	124-07-28-01-00-21
NASA–Ames Research Center Moffett Field, Calif. 94035	11. Contract or Grant No.
	13. Type of Report and Period Covered
12. Sponsoring Agency Name and Address	Technical Note
National Aeronautics and Space Administration Washington, D. C. 20546	14. Sponsoring Agency Code

15. Supplementary Notes

16. Abstract

Calculations of laminar heat transfer to windward wing and body surfaces of a straight wing MSC orbiter have been made at high angles of attack and with yaw. The predictions of heat transfer made by swept cylinder theory generally agree with measurements in areas free of external flow interference. An optimum elliptic cross section was then determined using swept cylinder theory for an aerodynamically heated windward body surface in radiation equilibrium.

17. Key Words (Suggested by Author(s))	18. Distribution Statement
Straight wing shuttle Aerodynamic heating, laminar flow Wing and body surfaces Angle of attack and yaw	Unclassified – Unlimited

19. Security Classif. (of this report)	20. Security Classif. (of this page)	21. No. of Pages	22. Price*
Unclassified	Unclassified	19	$3.00

*For sale by the National Technical Information Service, Springfield, Virginia 22151

SYMBOLS

B	pressure gradient parameter (eq. (8))
c	wing chord
h	static enthalpy
H	total enthalpy, $h + \frac{u^2 + v^2}{2}$
L	body length
M_∞	Mach number of free stream
p	pressure
P,Q,R,N	parameters in correlation function for $\frac{\theta'_w}{\theta'_{w,o}}$ (ref. 6)
$\dot{q}$	heat transfer per unit area
$\bar{q}$	heat-transfer coefficient, $\frac{\dot{q}}{h_{aw} - h_w}$
r	recovery factor, $\frac{h_{aw} - h_e}{H_e - h_e}$
R	body radius
R_S	reference sphere radius
s,y,z	crosswise, spanwise, and normal boundary-layer coordinates
t	enthalpy ratio, $\frac{h}{H_e}$
u,v,w	velocity components in s, y, and z-directions
U_b,V_b,W_b	velocity components in X_b, Y_b, and Z_b body directions (fig. 2)
U_w,V_w,W_w	velocity components in X_w, Y_w, and Z_w wing stagnation line coordinates
V_1	crossflow velocity (fig. 2)
V_∞	free-stream velocity
w	reference length (wing chord or body half-width)
$\frac{x}{c}$	chordwise distance

$\frac{x}{L}$	body distance
α	angle of attack
α_{bs}	effective body angle of attack with yaw (fig. 2)
α_{lb}	crossflow angle of attack (fig. 2)
α_{ws}	effective angle of attack of wing stagnation line
β	yaw angle of body (fig. 2)
γ	specific heat ratio
δ	dihedral angle of stagnation line in wing plane
δ_o	dihedral angle of wing plane
Λ	sweep angle of wing stagnation line
θ	angle between velocity vector and normal to body surface (eqs. (1) and (2))
$\frac{\theta'_w}{\theta'_{w,o}}$	enthalpy gradient ratio (eq. (5))
$\frac{\rho_2}{\rho_1}$	density ratio across shock wave

Subscripts

aw	adiabatic wall
e	edge of boundary layer
o	stagnation line value
w	wall
*	sonic value
∞	free-stream value

CALCULATION OF LAMINAR HEAT TRANSFER TO THE WINDWARD SURFACES OF STRAIGHT WING SHUTTLE VEHICLES AT HIGH ANGLE OF ATTACK AND WITH YAW

C. C. Pappas

Ames Research Center

SUMMARY

Calculations of laminar heat transfer to windward wing and body surfaces of a straight wing MSC orbiter have been made at high angles of attack and with yaw. The predictions of heat transfer made by swept cylinder theory generally agree with measurements in areas free of external flow interference. An optimum elliptic cross section was then determined using swept cylinder theory for an aerodynamically heated windward body surface in radiation equilibrium.

INTRODUCTION

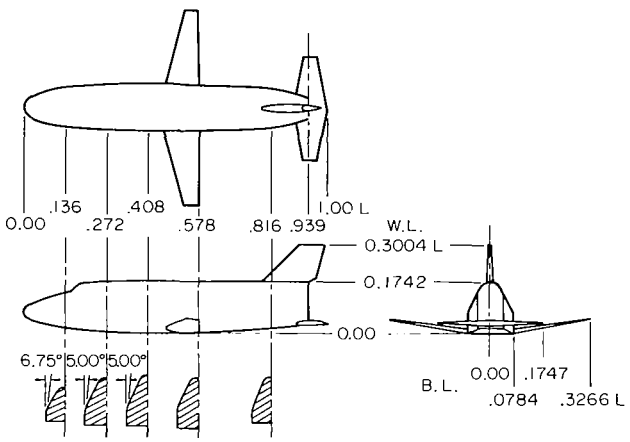

Figure 1.– Plan, elevation, and end view of MSC shuttle orbiter.

For the space shuttle vehicle the large booster vehicle will likely be of the low crossrange design and the smaller orbiter may be of low or high crossrange design, depending on requirements. An example of the low crossrange orbiter is the Manned Spacecraft Center (MSC) design shown in figure 1. Low crossrange reusable boosters may be of similar shape.

The task set forth in this report is to formulate a method for calculating the laminar-flow heating to the windward surfaces of a low crossrange orbiter during its reentry trajectory. The heat transfer to a body such as the MSC orbiter with its straight wing and essentially flat bottom appears amenable to calculation methods. The form that these calculations might take was decided as a result of viewing surface oil film flow patterns (examples of some of these are given later), obtained at high angles of attack and with yaw. These patterns indicate well-established surface flow emanating from the stagnation lines along the windward surfaces of the wing, elevon, and body and curving to the sides of the respective components. Thus, for the MSC orbiter, swept cylinder theory appears to be applicable with some degree of confidence in the areas free of external flow interference and where the body width or the wing chord does not vary too rapidly.

METHOD AND ANALYSIS

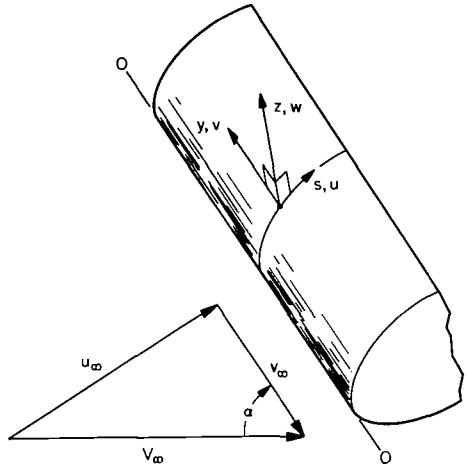

Sketch (a).– Coordinate system.

Consider, first, the vehicle windward surface to be locally cylindrical, but not necessarily circular or symmetrical, at high angle of attack and with a defined stagnation line 0–0 (see sketch (a)). The method of heat-transfer calculation requires knowledge of surface pressure, velocity, and velocity gradient at the edge of the boundary layer in the direction normal to the cylinder axis from the stagnation line to both sides of the vehicle (or to the leading and trailing edges of the wing). The stagnation line was located and the crossflow pressure distributions from the stagnation line to the sonic point were obtained for the body and wing cross sections. For the body cross sections the flat-face pressure distributions to the sonic point and velocity gradient at the stagnation line were obtained for the unyawed surface from Inouye (the method is briefly described in ref. 1) and from Bazzhin (ref. 2) for the yawed surface. The pressure distribution to the sonic point and the stagnation line velocity gradient for the wing cross section were obtained from Kaattari utilizing methods developed in reference 3. Beyond the sonic point, a modified Newtonian *pressure change* was used for a finite $\Delta\theta$ change followed by a Prandtl-Meyer expansion to the side of the body. The surface pressure at surface angle θ was obtained by one of the following equations. For the Newtonian part

$$\frac{p}{p_O} = \frac{p_*}{p_O} - (\cos^2 \theta_* - \cos^2 \theta) \tag{1}$$

is used when the side pressure ($\theta = 90°$) is unknown. For the case where a specified side pressure is to be matched to the Newtonian the pressure is

$$\frac{p}{p_O} = \frac{p_*}{p_O} - \frac{(\cos^2 \theta_* - \cos^2 \theta)}{\cos^2 \theta_*} \frac{\left(p_* - p_{side}\right)}{p_O} \tag{2}$$

The usual Newtonian method, $p/p_O = \cos^2 \theta$, is inadequate to predict the crossflow pressures for the flat faces and the wing cross sections. Also, surface pressures obtained by equations (1) and (2) agree better with measured values than pressures obtained from a Prandtl-Meyer (P–M) expansion from the sonic point. The P–M expansion initially underpredicts pressures beyond the sonic point. Love (ref. 4) applied the modified Newtonian pressure change initially from the sonic point and then the P–M expansion beyond to the shoulder; the $\cos^2\theta$ variation beyond the sonic point is matched to the P–M expansion where both agree, and the P–M expansion is continued to the shoulder of the body. A pressure gradient discontinuity is possible at the match point. Kaattari (ref. 5) also used a Newtonian variation beyond the sonic point, but assumed that the ideal Newtonian surface angle corresponded to $\cos^2 \theta = 0.5283$ ($\gamma = 1.4$, $\theta = 43.4°$) at the sonic point.

The change from the sonic point value is obtained as the value $0.5283 - \cos^2(43.4 + \Delta\theta)$. The methods of both Love and Kaattari agree quite well with measurement in their comparisons.

Once the pressure distribution was defined across the cylinder, the velocity distribution was obtained from the isentropic relation

$$\frac{u_e}{V_\infty} = \sin\alpha \left[1 + \frac{2}{(\gamma - 1)M_\infty^2 \sin^2\alpha}\right]^{1/2} \left[1 - \left(\frac{p}{p_o}\right)^{(\gamma-1)/\gamma}\right]^{1/2} \tag{3}$$

where α is the *effective* angle of attack of the stagnation line with respect to the free-stream velocity vector. The crossflow pressure distributions used were not always too accurate, with ensuing added inaccuracies in the velocity and velocity derivatives, especially at the stagnation line where a specified velocity gradient must be matched to fit the velocity curve. The result was inaccurate heat-transfer predictions near the stagnation line. Smoothings of the velocity distributions and corresponding adjustment of the pressure distributions were required to ensure more accurate heat-transfer predictions.

The inputs of p/p_o, u/V_∞, and $(du/V_\infty)/(ds/w)$ are utilized in the swept cylinder relations of Beckwith and Cohen (ref. 6) to give the heat-transfer coefficient ratios for the cold wall condition of high speed flow:

$$\frac{\bar{q}}{\bar{q}_o} = \left\{\frac{p}{p_o}\frac{t_o}{t}\frac{B_o}{B}\frac{(du/V_\infty)/(ds/w)}{[(du/V_\infty)/(ds/w)]_o}\right\}^{1/2} \frac{\theta'_w}{\theta'_{w,o}} \tag{4}$$

where

$$\frac{\theta'_w}{\theta'_{w,o}} = \frac{1 + PB^N}{Q + RB^N} \tag{5}$$

$$t_o = 1 - \cos^2\alpha \tag{6}$$

$$t = \frac{h}{H_e} = t_o - \left(\frac{u}{V_\infty}\right)^2 \tag{7}$$

$$B = \frac{2}{(u/V_\infty)^2} \frac{du/V_\infty}{ds/w} \frac{t_o}{t} \frac{p_o}{p} \int_o^{s/w} \frac{p}{p_o} \frac{u}{V_\infty} \frac{ds}{w} \tag{8}$$

Finally, the heat transfer relative to the stagnation value is

$$\frac{\dot{q}}{\dot{q}_o} = \frac{h_{aw} - h_w}{(h_{aw} - h_w)_o} \frac{\bar{q}}{\bar{q}_o}$$

which for a laminar recovery factor value of 0.85 becomes

$$\frac{\dot{q}}{\dot{q}_o} = \frac{1 - 0.15\cos^2\alpha - 0.15(u/V_\infty)^2 - [h_w/(V_\infty^2/2)]}{1 - 0.15\cos^2\alpha - [h_w/(V_\infty^2/2)]} \frac{\bar{q}}{\bar{q}_o} \tag{9}$$

The heat transfer is to be related to some reference value in the flight case, such as the stagnation-point heat transfer to a reference sphere. As noted in reference 7, the heat transfer to a swept circular cylinder is related to that of a sphere by the relation

$$\frac{\dot{q}_{o,cyl}\sqrt{R}}{(h_{aw} - h_w)_{o,\ circ\ cyl}} = 0.743 \frac{(\dot{q}_{o,\ sphere})_{V_\infty \sin\alpha}\sqrt{R}}{(H_e - h_w)_{o,\ V_\infty \sin\alpha}} \tag{10}$$

which becomes for the cold wall case where $h_w \to 0$

$$(\dot{q}_o)_{circ\ cyl} = 0.743(\dot{q}_{o,sphere})_{V_\infty \sin\alpha}(1 - 0.15\cos^2\alpha) \tag{11}$$

The form of this last relation is somewhat dependent on the form of the expression for the sphere heat transfer for flight conditions. Writing

$$\frac{(\dot{q}_o)_{body}}{(\dot{q}_o)_{sphere}} = \frac{(\dot{q}_o)_{body}}{(\dot{q}_o)_{swept\ circ\ cyl}} \frac{(\dot{q}_o)_{swept\ circ\ cyl}}{(\dot{q}_o)_{sphere}} \tag{12}$$

leads to the more useful expression

$$\frac{(\dot{q}_o)_{body}}{(\dot{q}_o)_{sphere}} = \left\{ \frac{[(du_e/V_\infty)/(ds/w)]_{o,body}\ (1/w)}{[(du_e/V_\infty)/(ds/R)]_{o,\ circ\ cyl}\ (1/R)} \right\}^{1/2} 0.743\sin\alpha(1 - 0.15\cos^2\alpha) \tag{13}$$

The final expression for the heat transfer on the wing or body relative to the sphere value is:

$$\frac{\dot{q}}{(\dot{q}_o)_{sphere}} = \frac{\dot{q}}{\dot{q}_o} \frac{\dot{q}_o}{(\dot{q}_o)_{sphere}} \tag{14}$$

The foregoing heat-transfer relations and crossflow pressure and velocity input data are obtained within certain limitations. First, the pressure distributions as used in this report were obtained for a perfect gas with constant $\gamma = 1.4$ and for the ideal gas density ratio across the normal shock wave. The crossflow pressure distribution on a *symmetrical* cylinder is little affected by real gas properties and density ratio at high velocity and altitude and tends to approach the modified Newtonian distribution at the high shock density ratios of flight. The effect of shock wave stand-off distance and density ratio on the velocity gradient at the stagnation point is small as can be shown in the following brief first-order argument in a two-dimensional stagnation region (see sketch (b))

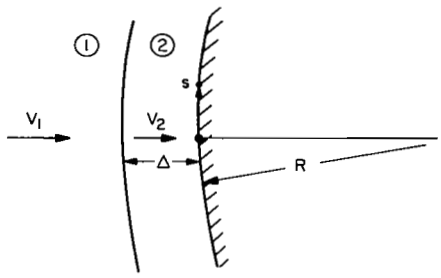

Sketch (b).– Two-dimensional stagnation region.

$$\frac{\partial u}{\partial s} = \left|\frac{\partial v}{\partial x}\right| \cong \frac{V_2}{\Delta} = \frac{\rho_1}{\rho_2}\,\frac{V_1}{\Delta} \tag{15}$$

$$\frac{\Delta}{R} = \frac{A(\text{const})}{(\rho_2/\rho_1) - 1}$$

for a circular cylinder

$$\frac{\partial u}{\partial s} = \frac{\rho_1}{\rho_2}\,\frac{V_1}{RA}\left(\frac{\rho_2}{\rho_1} - 1\right) = \frac{V_1}{RA}\left(1 - \frac{\rho_1}{\rho_2}\right) \tag{16}$$

The change in ρ_2/ρ_1 from 6 to a maximum near 18 results in a 13.3 percent increase in du/ds at the stagnation line. Again the velocity gradient enters the heat-transfer expression (eq. (13)) as the square root of the ratio of wing (or body) value to that of a circular cylinder at the same effective angle of attack, and both values are near equally affected by the shock density ratio. A more accurate analysis based on the results of Inouye (ref. 1) and Fuller (ref. 8) shows that the velocity gradient at the stagnation line of a circular cylinder actually decreases 34.7 percent over this same range of shock density ratios ($\rho_2/\rho_1 = 6$ to 18). However, the ratio of heat transfer on a flat-faced cylinder to that on a circular cylinder decreases only 11.5 percent for this variation in shock-density ratio. According to Cohen (ref. 7) the heat-transfer relation (eq. (10)) between a swept circular cylinder and a sphere should hold quite well for free-stream velocities below 8 km/sec. Therefore, the heat transfer to a swept symmetrical cylinder can be well represented by these calculations through the whole flight trajectory.

For a swept cylinder, such as a wing, that is not symmetrical about the stagnation line, a totally new problem can arise with increase in shock density ratio. The stagnation line will move to the position consistent with the shock wave lying nearer to the surface, changing both the stagnation line location and the stagnation line velocity gradient. A new flow pattern over the wing should be calculated conforming to the highest shock-density ratio of near 18 and for a new specific heat ratio, γ, behind the shock wave. The shock standoff distance then can be about 30 percent of the ideal value where $\rho_2/\rho_1 \cong 6$.

APPLICATION OF METHOD TO VEHICLE GEOMETRY

The body and wing axes and accompanying velocity vector components are illustrated in figure 2. Let V_∞ be the free-stream velocity at angle of attack α and yaw β.

$$\left.\begin{aligned} U_b &= V_\infty \cos\beta \cos\alpha \ , && \text{x-component body velocity} \\ V_b &= V_\infty \sin\beta \ , && \text{y-component body velocity} \\ W_b &= V_\infty \cos\beta \sin\alpha \ , && \text{z-component body velocity} \end{aligned}\right\} \tag{17}$$

$$V_1 = V_\infty(\sin^2\beta + \cos^2\beta \sin^2\alpha)^{1/2} \tag{18}$$

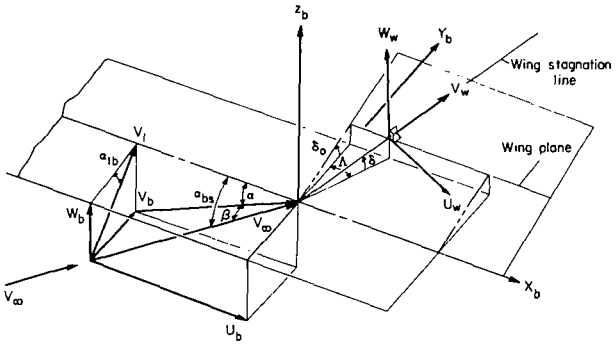

Vehicle coordinates and velocities

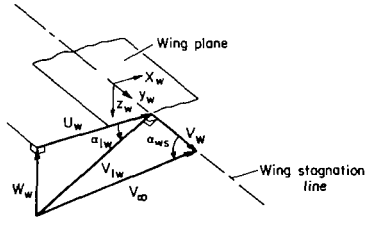

Wing coordinates and velocities

Figure 2.– Vehicle geometry and velocities.

is at angle $\alpha_{lb} = \tan^{-1}(W_b/V_b)$ with respect to x-y plane. The solution for the stagnation line location and pressure distribution of the crossflow on the bottom of the MSC body due to velocity V_1 depends on the angle α_{lb}. The velocity U_b is the sweep velocity along the X_b-body axis. The local angle of attack of the bottom surface is α:

$$\alpha = \alpha_{\text{body axis}} + (\Delta\alpha)_{\text{local}}$$

The detached body shock wave was considered to lie parallel to the body surface locally in the lengthwise direction. The crosswise pressure and velocity distributions were obtained from the detached shock-wave solutions of Inouye (ref. 1) for $\alpha_{lb} = 90°$ and from Bazzhin (ref. 2) for $\alpha_{lb} = 76°$ corresponding to the given yaw angle $\beta = 12.2°$. In later comparisons with measurements of heat transfer, the analytical approach can be evaluated for predicting heat transfer to the bottom body surface. The effective body angle of attack of the nonsymmetrical swept cylinder for cases with yaw β is defined as

$$\alpha_{bs} = \cos^{-1}(U_b/V_\infty) = \cos^{-1}(\cos\beta \cos\alpha)$$

The calculation of the heat transfer to the windward wing surface is somewhat more complicated. First, the stagnation line must be located along the windward wing surface at high angle of attack. For the straight wing orbiter with little leading-edge sweep, the chordwise wing cross section is considered at the local angle of attack. The detached shock wave and flow field are then defined for this two-dimensional flow, and the stagnation point is located. Assuming that the flow is similar across any of the spanwise locations, then the stagnation line is located at the two-dimensional chordwise position behind the swept leading edge. The free-stream velocity is then resolved with respect to the stagnation line.

Consider a wing plane (see fig. 2) at angle of attack α with dihedral angle δ_o, stagnation line sweep angle Λ, and body yaw angle β. The velocities U_w, V_w, W_w are components of the free-stream velocity V_∞ resolved with respect to the stagnation line in the wing plane

U_w component normal to the stagnation line in the wing plane

$$U_w = V_\infty \cos\beta \cos\Lambda \left(\cos\alpha \begin{matrix} L \\ \pm \\ R \end{matrix} \tan\beta \tan\Lambda\right) \tag{19}$$

where L denotes the upper sign for the left wing and R denotes the lower sign for the right wing.

V_w outward component parallel to the stagnation line in the wing plane

$$V_w = V_\infty \cos\beta \cos\delta \left(\cos\alpha \sin\Lambda + \sin\alpha \tan\delta \begin{matrix} L \\ \mp \\ R \end{matrix} \tan\beta \cos\Lambda\right) \tag{20}$$

W_w component normal to wing plane

$$W_w = V_\infty \cos\beta \cos\delta \left(-\cos\alpha \sin\Lambda \tan\delta + \sin\alpha \begin{matrix} L \\ \pm \\ R \end{matrix} \tan\beta \cos\Lambda \tan\delta\right) \tag{21}$$

The dihedral angle, δ, of the stagnation line in the wing plane is:

$$\delta = \tan^{-1}(\cos\Lambda \tan\delta_o)$$

The effective angle of attack of the wing plane with respect to the wing components of velocity is:

$$\alpha_{lw} = \tan^{-1}\frac{W_w}{U_w} = \tan^{-1}\left[\frac{\cos\delta\left(-\cos\alpha \sin\Lambda \tan\delta + \sin\alpha \begin{matrix} L \\ \pm \\ R \end{matrix} \tan\beta \cos\Lambda \tan\delta\right)}{\cos\Lambda\left(\cos\alpha \begin{matrix} L \\ \pm \\ R \end{matrix} \tan\beta \tan\Lambda\right)}\right] \tag{22}$$

For small sweep angles and dihedral angles of the stagnation line, α_{lw} is not much different from α. Now α_{lw} and V_{lw} determine the two-dimensional flow over a slightly modified chordwise wing cross section, which in turn provides the crossflow pressure and velocity distributions. The effective angle of attack of the wing stagnation line in the outward direction is defined as

$$\alpha_{ws} = \cos^{-1}\left[\cos\beta \cos\delta \left(\cos\alpha \sin\Lambda + \sin\alpha \tan\delta \begin{matrix} L \\ \mp \\ R \end{matrix} \tan\beta \cos\Lambda\right)\right] \tag{23}$$

For delta wings with highly swept leading edges the approach as outlined cannot be used directly but must be modified to account for the change in wing cross section as seen by the velocity vector $V_{lw} = V_\infty \sin\alpha_{ws}$ in order to establish the stagnation line location. As of now, there is not a readily available method to establish the stagnation line location, the pressure distribution and external velocity streamline path on a highly swept delta wing aircraft at high angle of attack

near 60°. However, the swept cylinder method was adapted in reference 9 to a 60° swept leading edge delta wing at 30° angle of attack with moderate success in predicting heat transfer along the chord at the 45.6 percent span position. The input of stagnation line location and crossflow pressure and velocity distributions require further refinement before adequacy of the method may be judged.

RESULTS AND DISCUSSION

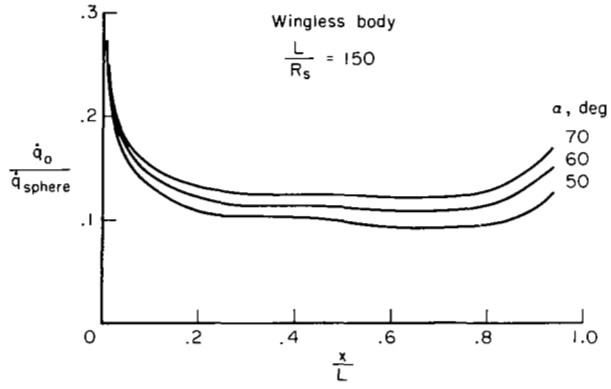

Figure 3.– Variation of predicted MSC orbiter fuselage centerline heating with angle of attack.

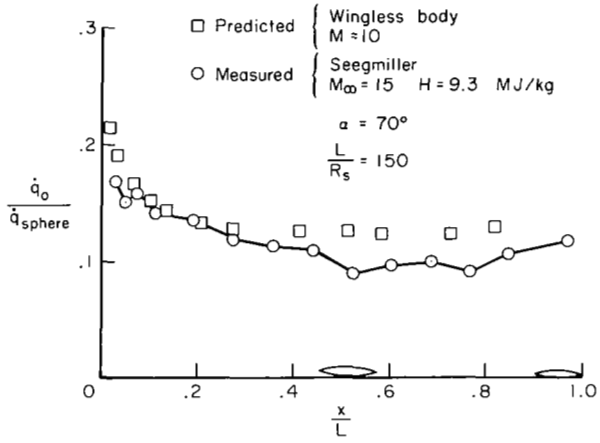

(a) $\alpha = 70°$

Figure 4.– Comparison of predicted and measured MSC orbiter fuselage centerline heating.

The heat transfer to the centerline of the windward body surface was calculated for a wingless MSC orbiter at the three angles of attack of 50°, 60°, and 70°. The heat transfer shown in figure 3 was referenced to that on a unit radius sphere where the length of the vehicle was 150 times the radius of the sphere or $L/R_S = 150$. The variation in heat transfer shown with x/L distance is due to the variation in local angle of attack of the body surface and the variation in body width as evidenced in equation (13). The shock envelope was assumed locally to lie parallel to the windward surface centerline. The crossflow velocity gradient for the flat surface was obtained from Inouye (ref. 1) and modified Newtonian flow was used for the circular cylinder value. Both were obtained at a normal Mach number of 10 using ideal gas properties.

Seegmiller (ref. 10) measured heat transfer to the MSC orbiter fuselage centerline in the Ames 42-Inch Shock Tunnel at a Mach number of 15. His measurements on the winged body are compared to the predicted values of the wingless body in figure 4. The measurements at angle of attack of 60° are from reference 10, but the measurements at 50° and 70° are unpublished. The measured heat transfer on the orbiter was referenced to that on a test sphere with $L/R_S = 24.5$, but is shown in figure 4 transformed to $L/R_S = 150$.

Fairly good agreement is obtained for the three angle-of-attack cases in the range of $0 < x/L \leqslant 0.45$, which is to a point just forward of the wing juncture. Near midchord of the wing the measured centerline heating rate drops, as expected, from 18 to 27 percent of the value just before the wing at $x/L = 0.44$ and then unexpectedly remains generally below the predicted values.

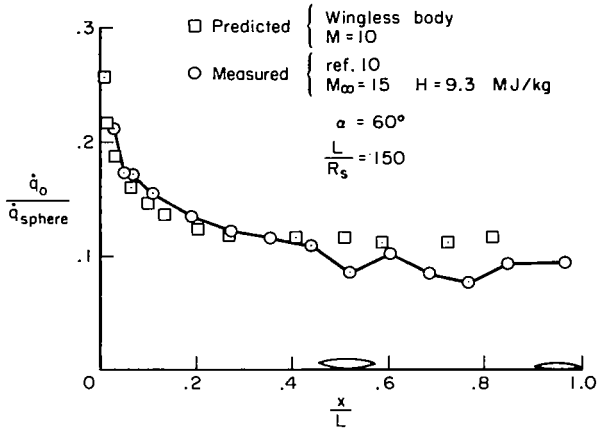

(b) $\alpha = 60°$

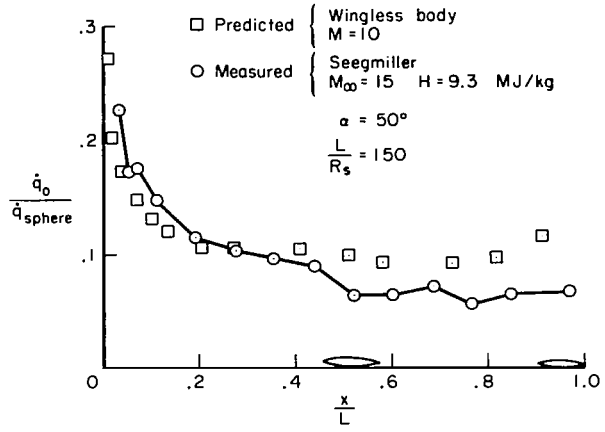

(c) $\alpha = 50°$

Figure 4.– Concluded.

The effect of the wing is to make the body effectively wider and to decrease $[(du_e/V_\infty)/(ds/w)](1/w)$ and the heat transfer to the body centerline. Surface oil flow paths show less streamline divergence away from the centerline, starting at midwing and extending aft. One would expect the measured heating to rise aft of the wing, but the measured trends are not systematic in behavior. However, for $\alpha = 70°$, the measured values increase gradually from the low point at $x/L = 0.52$ to $x/L = 0.87$. For the case $\alpha = 60°$, the measured heating just aft of the wing increased almost to the predicted value then fell again to values near that of the wing midspan. For $\alpha = 50°$, the measured values aft of the wing remain low at the heating value near the wing midspan.

The centerline and outer edge heating rates on the MSC orbiter are shown in figure 5 along the windward body surface. The lateral variation in heating from the centerline for $\alpha = 60°$ is greater than the change in heating due to angle-of-attack change from 50° to 70°. Comparison of the measured lateral heating on the bottom surface is made in figure 6, where the present theoretical

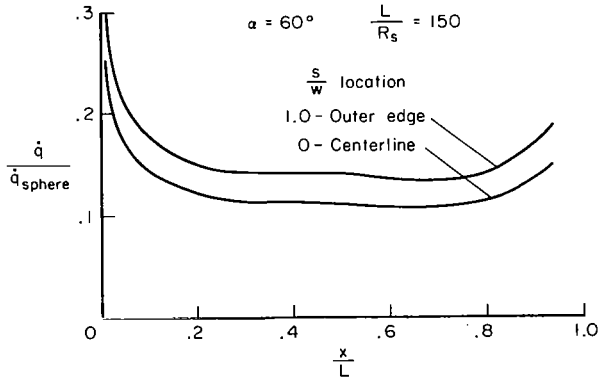

Figure 5.– Centerline and outer edge heating on MSC orbiter windward fuselage surface.

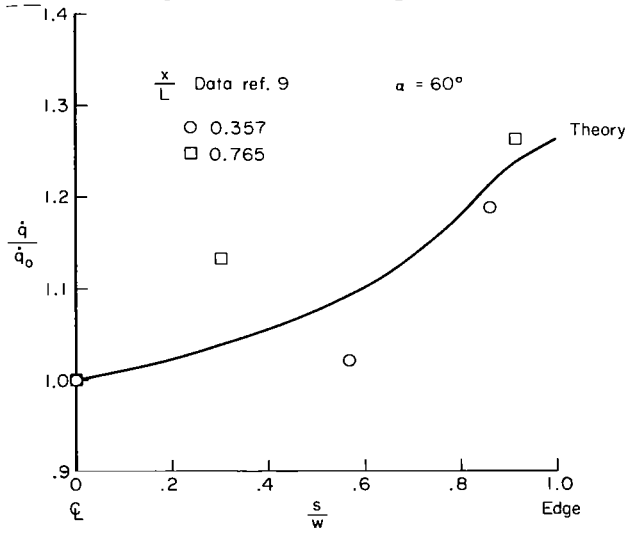

Figure 6.– Lateral heating distribution on MSC orbiter windward body surface.

prediction for the flat face with a sharp corner is compared with some data obtained by Seegmiller (ref. 10) at 60° angle of attack. The theory generally predicts the trend in the measurements. The data are from two body stations, one in the undisturbed flow ahead of the wing, and the other midway between the wing and elevon where disturbances in the flow may be present. More data are required to confirm the theoretical predictions.

Surface flow lines are shown for the MSC orbiter at two angles of attack and yaw in figure 7. These pictures (obtained from reference 11) clearly show the well-defined stagnation lines that exist on the windward wing and body surface as in figure 7(a). This supports the idea that crossflow theory may be applied to such bodies at high angles of attack and with yaw. Figure 7(b) shows that for the lower angle of attack and greater yaw, interference regions of flow near the wing juncture are more severe and that the body shock wave impingement on the bottom left wing creates a rather large interference region where crossflow theory is inappropriate. Measurements of the body

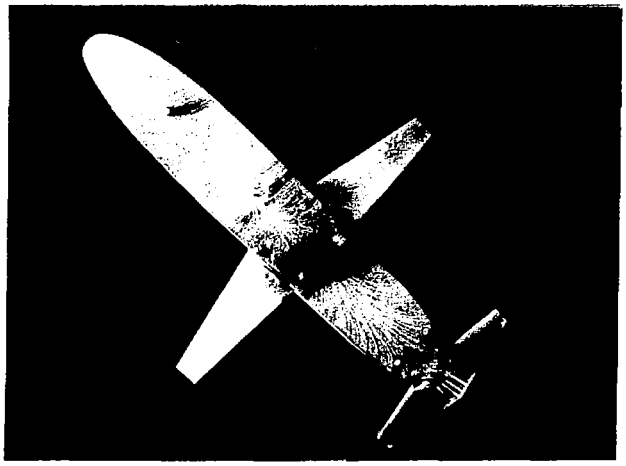

(a) $\alpha = 75°$ and $\beta = 5°$

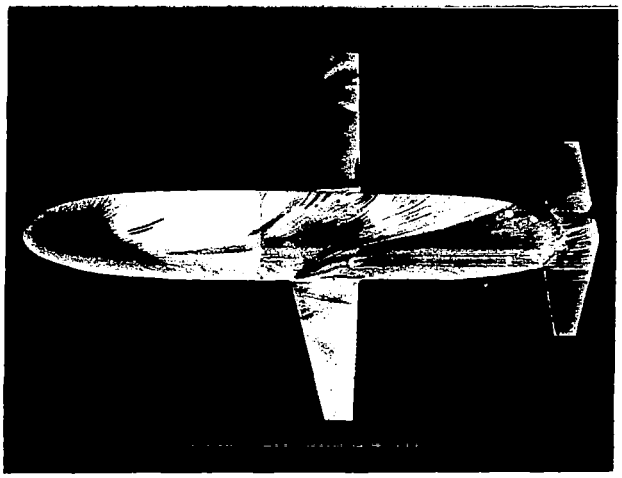

(b) $\alpha = 50°$ and $\beta = 10°$

Figure 7.– Surface flow lines at angle of attack and yaw.

stagnation line shift due to yaw were made at x/L = 0.325 and plotted as a function of the crossflow angle of attack α_{lb}. These measurements are compared with the results of Bazzhin in figure 8. The measurements show a greater displacement of the stagnation line especially at the higher α_{lb} values. Also some three-dimensional effects emanating from the body nose are influencing the stagnation line location for this x/L position.

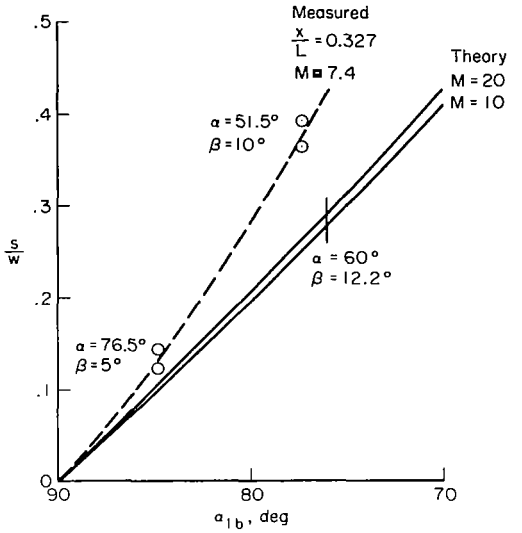

Figure 8.— Stagnation line shift on windward body surface due to yaw angle.

The effect on the heat transfer of yawing a flat-faced body with sharp corners is shown in figure 9. The theoretical predictions of heat transfer were made using the crossflow pressure

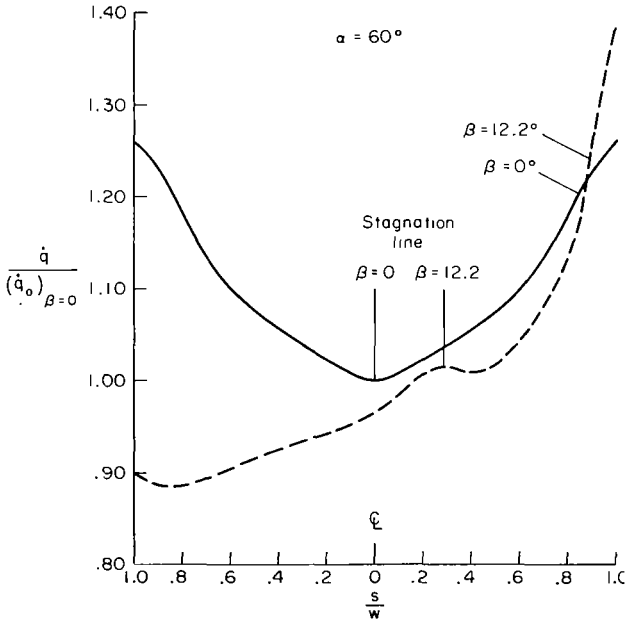

Figure 9.— Lateral heat-transfer distribution on flat-faced body with yaw.

distributions of Inouye (ref. 1) for zero yaw and of Bazzhin (ref. 2) for yaw angle of 12.2°. The peak heating at the corner with yaw is increased over the zero yaw value by 10 percent but the overall heating load is obviously less. A slight increase in the stagnation line heating is also evident with yaw. As mentioned in the preceding section, the theoretical calculation of the heat transfer near the stagnation region may show irregular behavior when the accuracy of the crossflow input data of pressures and velocities is not exact. This was the situation for the Bazzhin data most of which was obtained from not too well-defined curves. The Inouye data were from numerical listings and cause no apparent irregularity in the heat-transfer predictions.

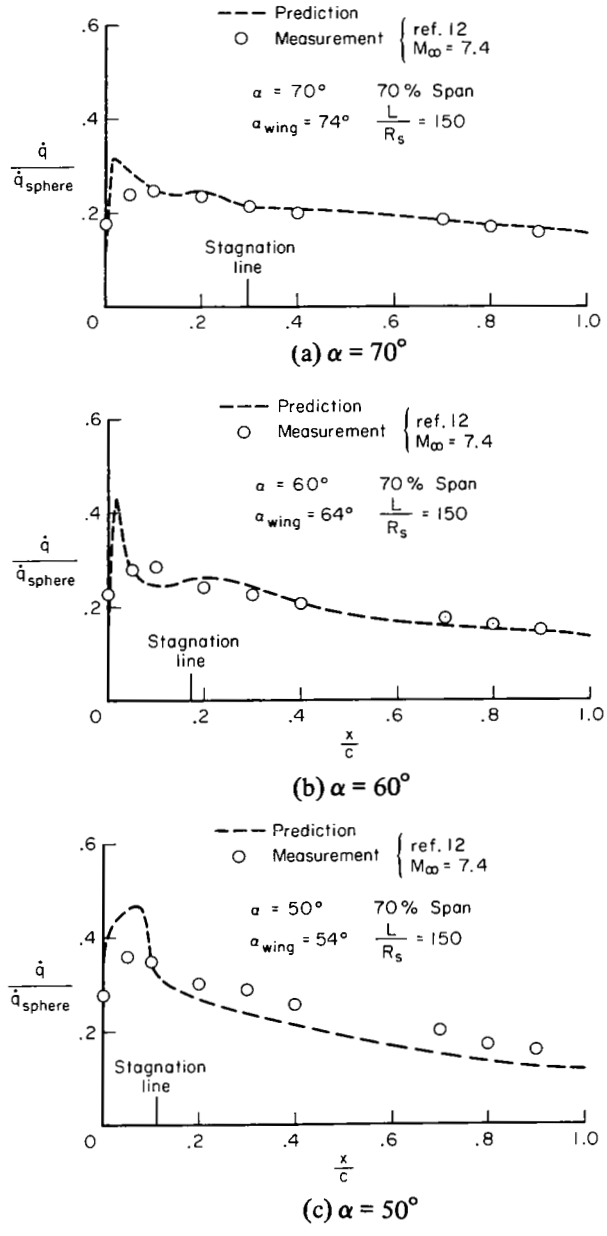

Figure 10.– Comparison of predicted and measured heat transfer to the MSC orbiter windward wing surface.

Predictions of the heat transfer on the windward surface of the MSC orbiter wing for three angles of attack are compared in figure 10 with the measurements made by Seegmiller (ref. 12) in the Ames 3.5-Foot Wind Tunnel. For the high angle of attack, $\alpha = 70°$ (fig. 10(a)) there is excellent agreement between theory and measurement except for one measurement at the 5-percent chord position, where the theory shows a sharp rise in heat transfer as the flow expands around the leading edge of the wing and then a decrease to the leading-edge value.

Quite good agreement between theory and experiment is again shown in figure 10(b) for the angle of attack $\alpha = 60°$. The theory predicts a peak value at $x/c \cong 0.02$ which was not detected by the experiment because of the limited number of thermocouples in the region.

A final comparison of wing heating is made in figure 10(c) at angle of attack $\alpha = 50°$. Here the theory uniformly underpredicts the measured heat transfer aft of the stagnation line and overpredicts ahead of the stagnation line. The reason for this greater disagreement at 50° angle of attack is not apparent. A reexamination of the crossflow pressure and velocity data may be in order.

A final examination of the effects of yaw angle on the wing heat transfer is shown in figure 11 for the MSC orbiter at 60° body angle of attack and 12.63° angle of yaw. One result of the calculations was that α_{lw} (wing angle of attack in the wing coordinate system)

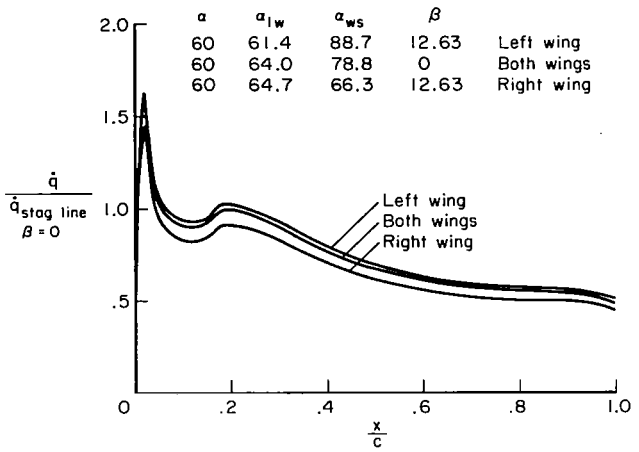

Figure 11.– Effect of yaw angle on the heat transfer to the MSC orbiter wing.

did not vary appreciably from the zero yaw value of $\alpha_{lw} = 64°$; therefore the same crossflow pressure and velocity distributions were used in the evaluation of the chordwise heat-transfer variation. In general, each of the three values of α_{lw}, one for the left and one for the right wing with yaw, and one for both wings at zero yaw, requires a separate determination of the input crossflow pressures and velocities to determine the chordwise heat-transfer distribution. Together with α_{lw}, which also determines the stagnation line velocity gradient, α_{ws} determines the effect of sweep velocity on the heat transfer to the wing. The overall effect is a 9-percent decrease in heat transfer for the right wing and a 3-percent increase for the left wing.

The present methods for calculating laminar heating were applied to determine an optimum elliptic body shape that ensures the maximum extent of uniform heating across the windward surface. For a radiation cooled surface, which is of minimum thermal capacity, uniform heating results in uniform temperature across a body surface in radiation equilibrium. The heat transfer to the various elliptic body shapes, with major to minor axis ratios a/b = 1.0 (circular cylinder), 1.5, 2.0, 3.0, and ∞ (flat face), all at 60° angle of attack, is compared in figure 12 to the stagnation line heat transfer of the circular cylinder. An elliptic cylinder with a/b value near 2.5 would give the maximum extent of uniform heating from the stagnation line, but it would not be the minimum total heating to the body windward side. Other calculations show that the heat-transfer ratios change very little with angle of attack in the range from 40° to 90°. The crossflow pressure distributions on the elliptic cylinders and other details of the calculations which enter into the results of figure 12 are given in reference 13.

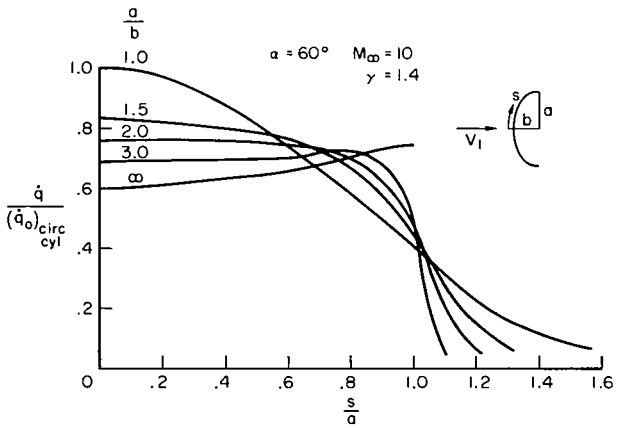

Figure 12.– Heat transfer to elliptic cylinders compared to circular cylinder.

CONCLUDING REMARKS

A method is presented to calculate the laminar heating on the windward surfaces of the space shuttle straight wing orbiters (or boosters) at high angles of attack and with yaw.

From the results of this report it can be concluded that the laminar heat transfer to the windward surfaces of the MSC orbiter can be calculated by swept cylinder laminar boundary-layer theory to an adequate accuracy. The method is applicable in areas where external flow interference is minimal and at angles of attack of 50° to 90° and with yaw.

For a windward body surface in radiation equilibrium, the maximum extent of temperature uniformity may be achieved with an elliptic cross section having a major to minor axis ratio of near 2.5.

The success of the method in predicting windward surface heat transfer also suggests that swept cylinder boundary-layer theory might be useful for calculating a transition criterion based on momentum or displacement thickness Reynolds number. Such an application has to be tested experimentally.

Ames Research Center
National Aeronautics and Space Administration
Moffett Field, Calif., 94035, Jan. 21, 1972

REFERENCES

1. Inouye, M.; Marvin, J. G.; and Sinclair, A. R.: Comparison of Experimental and Theoretical Shock Shapes and Pressure Distributions on Flat Faced Cylinders at Mach 10.5. NASA TN D–4397, 1968.

2. Bazzhin, A. P.: On Calculation of Supersonic Flow of Gas Over a Thin Plate With a Detached Shock Wave. *Engineering J.*, no. 2, 1963, pp. 31-39.

3. Kaattari, George E.: A Method for Predicting Shock Shapes and Pressure Distributions for a Wide Variety of Blunt Bodies at Zero Angle of Attack. NASA TN D–4539, 1968.

4. Love, E. S.; Woods, W. C.; Rainey, R. W.; and Ashby, G. C., Jr.: Some Topics in Hypersonic Body Shaping. 7th AIAA Aerospace Sciences Meeting, New York, N. Y., Jan. 20-22, 1969.

5. Kaattari, George E.: A Method for Predicting Pressures on Elliptic Cones at Supersonic Speeds. NASA TN D–5952, 1970.

6. Beckwith, Ivan E.; and Cohen, Nathaniel B.: Application of Similar Solutions to Calculation of Laminar Heat Transfer on Bodies With Yaw and Large Pressure Gradient in High Speed Flow. NASA TN D–625, 1961.

7. Cohen, Nathaniel B.: Boundary-Layer Similar Solutions and Correlation Equations for Laminar Heat-Transfer Distribution in Equilibrium Air at Velocities up to 41,000 Feet Per Second. NASA TR R–118, 1961.

8. Fuller, Franklyn B.: Numerical Solutions for Supersonic Flow of an Ideal Gas Around Blunt Two-Dimensional Bodies. NASA TN D–791, 1961.

9. Marvin, J. G.; Seegmiller, H. L.; Lockman, W. K.; Mateer, G. G.; Pappas, C. C.; and DeRose, C. E.: Surface Flow Patterns and Aerodynamic Heating on Space Shuttle Vehicles. AIAA Paper 71–594, AIAA 4th Fluid and Plasma Dynamics Conference, Palo Alto, Calif., June 21-23, 1971.

10. Seegmiller, H. Lee: Space Transportation System Technology Symposium. Vol. I. Aerothermodynamics and Configurations. NASA TM X–52,876, 1970, pp. 142-193.

11. Seegmiller, H. Lee: Shadowgraphs and Surface-Flow Visualization Photographs of the MSC Orbiter at M = 7.4. NASA TM X–62,032, 1971.

12. Seegmiller, H. Lee: Shock Interference Heating and Density-Ratio Effects. Part I – Flow Field Visualization, Thermocouple Measurements, and Analysis. NASA TM X–2272, 1971, pp. 185-215.

13. Pappas, C. C.: Windward Body Surface Study for Laminar Heating of Space Shuttle Vehicles at High Angle of Attack. NASA TM X–62,075, 1971.

NASA-Langley, 1972 — 1 A-4196